Am J Transl Res 2024;16(1):85-97
www.ajtr.org /ISSN:1943-8141/AJTR0153649

Original Article

Mapping the epitope of PD-L1 to the paratope of the antibody durvalumab using molecular dynamics simulation

Wenjian Tu[1,2]

[1]*School of Biology and Biological Engineering, South China University of Technology, Higher Education MegaCenter, No. 382 East Outer Loop Road, Guangzhou 510006, Guangdong, China;* [2]*Guangdong Vocational Institute of Sport, Guangzhou 510663, Guangdong, China*

Received September 26, 2023; Accepted December 12, 2023; Epub January 15, 2024; Published January 30, 2024

Abstract: Objectives: Durvalumab, a human monoclonal antibody that stops PD-L1 from attaching itself to CD80 and PD-1, was approved by the Food and Drug Administration for use in cancer therapy. An essential stage in antibody optimization is mapping paratope residues to epitope residues. In this study, our earlier computer-aided method based on molecular dynamics (MD) simulations was used to observe the paratope residues on durvalumab and their companions on PD-L1. Methods: The durvalumab/PD-L1 complex model was obtained from the Protein Data Bank and used in a rectangular box for solvation. On durvalumab, the paratope residues and their companions on PD-L1 were identified using MD simulations. The interface residues were ranked on the basis of their contributions to the binding of durvalumab and PD-L1 by assessing the stability of hydrogen bonds and salt bridges. This assessment was conducted using free and guided MD simulations. Results: Seventeen residues, including ASP26, GLU58, GLU60, ASP61, ARG113, ARG125, and THR127 on PD-L1 and H31ARG, H52LYS, H53GLN, H57GLU, H99GLU, H103PHE, H113ARG, L28ARG, L31SER, and L92TYR on durvalumab, were expected to be necessary for the binding of durvalumab to PD-L1. ASP26, ARG113, and ARG125 on PD-L1 were essential for its binding to PD-1. Eight residues (GLU60, ASP61, and THR127 on PD-L1 and L31SER, H99GLU, H53GLU, H31ARG, and H113ARG on durvalumab) were newly found, and two residues (LYS124 on PD-L1 and L94SER on durvalumab) proven nonessential for complexation, compared to the findings from the examined crystal structure. Conclusions: The antithrombotic antibody of durvalumab's paratope may be effectively mapped to the PD-L1 epitope using the existing computer method. This information will help optimize durvalumab.

Keywords: Durvalumab, PD-L1, paratope, epitope, MD simulations

Introduction

Blocking the connection between programed death ligand 1 (PD-L1) and PD receptor 1 (PD-1) is currently the most promising approach for cancer treatment [1-3]. PD-1 is a transmembrane protein, categorized as type I, comprising 288 amino acids. It is predominantly found on the surface of activated T cells in peripheral organs. Conversely, the PD-L1 protein, which is also a type I transmembrane protein, comprises 290 amino acids and is primarily synthesized by macrophages and dendritic cells [4, 5]. However, the frequent PD-L1 overexpression in various cancer types enables carcinomas to evade the host's immune system when combined with PD-1 [6]. Therefore, disruption of interactions between PD-1 and PD-L1 can restore the immune response, making PD-1 and PD-L1 promising targets for cancer immunotherapy [1, 7, 8].

Over the last several years, therapies that inhibit PD-1/PD-L1 using antibodies have shown amazing potential [7, 9, 10]. Pembrolizumab and nivolumab, as anti-PD-1 medications, have been extensively used for various malignancies since 2014 and have shown excellent therapeutic effects [9, 11]. Atezolizumab was the first Food and Drug Administration (FDA)-approved anti-PD-L1 drug (2016) and was designated for the treatment of advanced urotheli-

https://doi.org/10.62347/ISDD4626

Table 1. Identified interaction residues between PD-1 with PD-L1 by molecular dynamics simulation

PD-1	PD-L1
ASN66, TYR68, GLN75, LYS78, ALA132, GLU136	ASP26, GLN66, ARG113, ALA121, ASP122, TYR123, ARG125

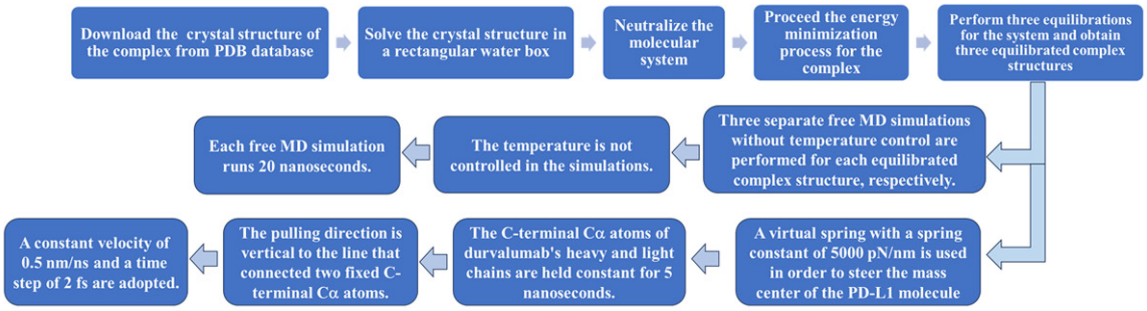

Figure 1. Flow chart of free and steered MD simulations. MD, molecular dynamics.

al carcinoma and metastatic non-small-cell lung cancer [12, 13]. In 2017, the FDA also approved the anti-PD-L1 drugs, durvalumab and avelumab, for treating advanced bladder cancer and Merkel cell carcinoma [14].

The human monoclonal antibody, durvalumab, sometimes referred to as MEDI4736, inhibits the interaction between PD-L1, CD80, and PD-1 [15]. Despite being approved by the FDA for use in cancer treatment, multiple Phase III clinical trials are still ongoing in non-small-cell lung cancer, head and neck cancer, and urothelial cancer [16]. However, the molecular basis of durvalumab-based anti-PD-L1 reactivity and binding properties compared with other anti-PD-L1 antibodies used in clinics, such as avelumab and BMS-936559, is yet to be clearly elucidated [17]. To begin this process, paratope residues must be mapped to epitope residues [18]. The durvalumab/PD-L1 complex's crystal structure has been explained, and details of epitope-paratope residue interactions at the atomic level were provided in 2017 [14]. However, protein recognition is a dynamic process and often fails to indicate the importance of these residue interactions during binding [19, 20]. Therefore, protein dynamics and other processes were assessed using molecular dynamics (MD) simulations, such as protein folding and complex dissociation [21, 22]. MD modeling is used to determine the most significant residues in the PD-1/PD-L1 complex interaction (**Table 1**) [23]. It has also proven to be an efficient tool in mapping paratopes to epitopes for therapeutic antibodies, such as 6B4, 10B12, and pembrolizumab, with high sensitivity, high specificity, and low false positive rate [20, 23, 24].

Therefore, using our earlier computer-aided method based on MD simulations, the paratope residues on durvalumab and their companions on PD-L1 were examined [20]. Seventeen residues, including ASP26, GLU58, GLU60, ASP61, ARG113, ARG125, and THR127 on PD-L1 and H31ARG, H52LYS, H53GLN, H57GLU, H99GLU, H103PHE, H113ARG, L28-ARG, L31SER, and L92TYR on durvalumab, were predicted to play an essential role in durvalumab binding to PD-L1. ASP26, ARG113, and ARG125 on PD-L1 were proved to be crucial for its binding with PD-1 (**Table 1**), suggesting that durvalumab prevents PD-1 from interacting with PD-L1 because of steric hindrance. GLU58, GLU60, and ASP61 on PD-L1 were predicted to be critical residues for the binding between PD-L1 and the antibody avelumab [25]. GLU58 was an epitope residue in the BMS-936559/PD-L1 complex's interface [10]. Information on the remaining 11 residues is limited. Further confirmation using mutagenesis experiments is necessary. These residues are potential targets to improve the efficacy of the antibody durvalumab, and our MD simulation-based computer-aided approach can guide antibody designs and mutagenesis studies.

Methods

Simulations in both free and guided MD formats

A flowchart of the free and guided MD simulations is shown in **Figure 1**. VMD [26] and NAMD

2.9 [27] are the software packages used for MD simulations and visualization and modeling, respectively. Using the code 5X8M, the crystalline structure of PD-L1 attached to durvalumab was obtained from the protein data library. It was solved in a 7.68 nm × 12.58 nm × 8.03 nm rectangular box using water molecules that included TIP3P as a solvent. Next, 150-mM NaCl was added to neutralize the system. The all-atom force field CHARMM22 [28], a periodic boundary condition, cMAP correction of the backbone, the Ewald technique for the electrostatic interaction particle mesh, and a cutoff of 12 Å for the electrostatic and van der Waals interactions were all used. A time step of 2 fs was used for the MD simulations. Two phases were involved in the minimization process. Within the first 15,000 stages of the system's energy minimization process, every atom of the protein was locked in place. After the atoms were released, a further 15,000 steps of minimization were performed. Then, the system was brought three times to 20 ns of pressure and temperature equilibrium. Langevin dynamics was used to maintain the temperature at 310 K. In addition, the Langevin piston method was used to maintain the pressure at 1 atm. To monitor the equilibrium state of the three systems, variations in the root mean square deviation (RMSD) of the heavy atoms were considered. Three equilibrated complex structures were chosen from three related equilibrations as the three beginning conformations for subsequent unsupervised and supervised MD simulations.

For every difficult structure that was stable, three separate and guided MD simulations were performed. The survival rates of the bonds in the interface were measured after a 20-ns free MD simulation without temperature or pressure controls. A virtual spring with a spring constant of 5000 pN/nm was used to steer the mass center of PD-L1 molecules. This spring was created by linking a dummy atom to a steered atom. During guided MD simulations, the C-terminal C_α atoms of durvalumab's heavy and light chains were kept constant. The antibody durvalumab was stopped for 5 ns while moving at a constant velocity of 0.5 nm/ns and a time step of 2 fs. The direction in which it moved was vertical to the line connecting the two fixed C-terminal C_α atoms. For every equilibrated structure, three directed MD simulations were conducted, and the bond breakage times under stretching at the interface were determined.

The Guangzhou National Supercomputer Center assisted with these simulations.

Normalized rupture time, stability index, and survival ratio of hydrogen bonds

When classifying paratope-to-epitope residues, the most stable salt bridges and/or bonds at the interface could be utilized [20, 29]. When the bonding angle and the distance between the donor and acceptor were less than 30 degrees and < 3.5 Å, respectively, a bond was observed. Salt bridges were examined using a bond length threshold of 3.5 Å. VMD software was used to find the bonds across a complicated interface [23, 30]. The likelihood that a bond will continue to exist is represented by the ratio (ω) of the amount of time it has survived to the amount of time that it has been simulated. As long as the link survives throughout the simulation period, the bond has a rupture time.

Within the free MD simulations, the thermal stability of a bond is represented by its survival ratio (ω_j) for the *j*th bond. This ratio was calculated for each bond. ω_j is the maximum value of ω_{j1}, ω_{j2}, and ω_{j3}, and ω_{ji} (i = 1, 2, and 3) is the mean survival ratio of the *j*th bond derived from three separate MD simulations using the *i*th initial equilibrated complex conformation. In directed MD simulations, the comparative tensile force that the *j*th bond exhibits under mechanical stress was correlated with the normalized rupture time α_j. $\alpha_j = \theta_j/\max\{\theta_1, \theta_2, ..., \theta_N\}$ and $\theta_j = \max\{\theta_{j1}, \theta_{j2}, \theta_{j3}\}$, where N is the total number of bonds being considered and θ_{ji} is the mean rupture time of the *j*th bond determined from three guided MD simulations using the *i*th initial equilibrated complex conformation for i = 1, 2, and 3, respectively. The stabilization index of the *j*th bond, abbreviated as $HBSI_j$, is defined as $HBSI_j = \max(\omega_j, \alpha_j)$, combining the effects of the thermal stability and mechanical strength of the bond on the paratope-epitope interactions. In contrast to the findings of our earlier study [20], in which the mean survival ratio and normalized rupture time were defined as the HBSI value, the maximum mean survival ratio and normalized rupture time were adopted here [23]. This is because a bond may only be thermally or

Table 2. Residue interactions between PD-L1 and durvalumab in crystal structure

No.	Hydrogen bond				Salt bridge	
	PD-L1		Durvalumab		PD-L1	Durvalumab*
	Residue	Atom	Residue*	Atom	Residue	Residue
1	ARG113	NH2	H57GLU	OE2	ASP26	L28ARG
2	LYS124	NZ	L94SER	OG	ARG113	H57GLU
3	ARG125	NH1	L92TYR	O	GLU58	H52LYS
4	ARG125	NE	H103PHE	O		

*The name of the residues involving in hydrogen bonds or salt bridges with H or L indicating that the residues are on the heavy or the light chain of durvalumab, respectively, and with the number indicating the position of the residue (first three-letter amino acid code).

mechanically stable. For example, bonds 7, 10, and 11 in **Table 3** appeared only in free MD simulations. In contrast, the No. 24-30 bonds in **Table 3** appeared only in the guided MD simulations. Moreover, the mechanical stretch in the guided MD simulation could induce a large conformational transformation of the complex interface, and some potentially vital interactions could only be detected in that scenario. Therefore, this correction ensured that thermally or mechanically stable bonds could be sorted out, and all possible interaction-residue pairs in the interface were provided. Any survival ratio, normalized rupture time, or HBSI index that falls between the ranges of 0-0.3, 0.3-0.55, or 0.55-1.0, respectively, which is considered normal, indicates poor, moderate, or high stability for a bond, respectively [20, 29].

Results

Crystal structures provided less information on the interaction between residue pairs at the interface

The PD-L1/durvalumab complex's crystal structure showed three salt bridges and four bonds spanning the complex interface (**Table 2**). These seven bonds were contributed by five residues, ASP26, GLU58, ARG113, LYS124, and ARG125, on PD-L1 and their respective partners, L28ARG, H52LYS, H57GLU, L94SER, L92TYR, and H103PHE, on durvalumab (**Table 2**).

Among these five epitope residues on PD-L1, ASP26, ARG113, and ARG125 were critical for its binding with PD-1 (**Table 1**). ASP26 and ARG113 each formed one hydrogen bond with PD-1, whereas ARG125 formed six hydrogen bonds [23]. This implied that durvalumab prevents PD-1 from interacting with PD-L1 because of steric hindrance. However, because conformation transformation is entirely overlooked, and protein recognition is a dynamic process, only seven bonds were found, and the frozen crystal structure may give some of the contact residues. Therefore, MD simulations were conducted to explore other interaction residues and to test the strength of the bonds at the interface.

Reciprocity mapping from the paratope to the epitope is achieved by the thermal stabilization of bonds

It was postulated that paratopes and epitopes could establish bonds with exceptional thermal stability through free MD simulations [20]. Initially, the PD-L1/durvalumab complex was brought into equilibrium thrice using an identical energy minimization protocol (Methods). The RMSD time profiles for the heavy atoms (**Figure 2**) indicated that the three systems' equilibration occurred after a 5-ns duration. By conducting free MD simulations for 20 ns on each of the initial conformations I, II, and III after equilibration of the PD-L1/durvalumab complex, the bond formation and disruption were analyzed. The survival ratios of the identified bonds are detailed in **Table 3**. In contrast to the crystal structure analysis results shown in **Table 2**, the consolidated findings in **Table 3** encompass the discovery of 16 additional bonds. The seventh detected bond was exclusively observed in the simulations related to the equilibrated conformation II. Conversely, the tenth and eleventh identified bonds were present in simulations of equilibrated conformations I and II (**Table 3**). Because of the initial state-dependent binding formation characteristics, several parallel simulations are neces-

Table 3. Summary of survival ratios, rupture time, and involved residues of hydrogen bonds detected from free and steered MD simulations

Bond	Bond	PD-L1		Durvalumab		Survival ratio			Rupture time (ns)		
No	Type	Residue	Atom	Residue*	Atom	I	II	III	I	II	III
1	H	ARG113	NH2	H57GLU	OE1	0.97±0.02	0.97±0.01	0.66±0.49	2.97±1.20	2.39±0.44	3.02±0.51
2	S	GLU58		H52LYS		0.89±0.10	0.96±0.05	0.93±0.11	3.33±1.37	0.02±0.01	0.03±0.01
3	S	ARG113		H113ARG		0.94±0.02	0.94±0.02	0.94±0.02	3.22±1.01	0.02±0.00	0.04±0.01
4	H	ARG113	NH1	H57GLU	OE2	0.78±0.06	0.86±0.02	0.57±0.50	2.72±1.05	1.86±0.47	3.28±0.69
5	H	ARG125	NH1	L92TYR	O	0.64±0.25	0.79±0.06	0.79±0.09	2.16±0.98	0.90±0.42	2.30±0.29
6	H	ARG125	NE	H103PHE	O	0.46±0.20	0.75±0.06	0.72±0.10	0.48±0.42	0.01±0.00	0.21±0.35
7	S	ASP26		L28ARG		-	0.48±0.17	-	-	-	-
8	H	GLU58	OE2	H52LYS	NZ	0.35±0.13	0.46±0.06	0.37±0.12	1.01±0.31	0.73±0.34	1.23±0.49
9	H	ARG125	NH2	H103PHE	O	0.44±0.18	0.18±0.09	0.21±0.10	1.39±0.65	0.59±0.37	1.91±0.09
10	H	ASP26	OD1	L28ARG	NH2	0.17±0.17	0.42±0.26	-	-	-	0.18±0.31
11	H	ASP26	OD2	L28ARG	NH1	0.06±0.06	0.40±0.25	-	-	-	-
12	H	GLU58	OE1	H52LYS	NZ	0.37±0.10	0.33±0.05	0.39±0.07	1.64±0.77	0.88±0.22	1.14±0.28
13	H	ASP26	OD2	L31SER	N	0.20±0.13	0.39±0.08	0.26±0.19	0.52±0.85	0.15±0.25	0.03±0.05
14	H	GLU60	O	H53GLN	NE2	-	0.07±0.06	0.38±0.37	0.03±0.06	0.03±0.05	0.29±0.29
15	H	ARG113	NH1	H57GLU	OE1	0.02±0.00	0.01±0.00	0.32±0.51	-	-	-
16	H	ASP26	OD1	L31SER	N	0.18±0.03	0.29±0.10	0.12±0.11	1.30±0.67	0.59±0.29	1.82±1.45
17	H	ASP26	OD2	L28ARG	NH2	0.14±0.12	0.29±0.06	0.00±0.01	-	-	-
18	H	ASP26	OD1	L28ARG	NH1	0.10±0.09	0.27±0.05	-	-	-	-
19	H	ARG113	NH2	H57GLU	OE2	-	-	0.24±0.40	-	-	-
20	H	TYR123	OH	H50ASN	ND2	0.23±0.24	0.07±0.05	0.06±0.10	0.77±0.58	0.24±0.26	0.83±0.73
21	H	ASP26	OD2	L31SER	OG	0.04±0.04	0.01±0.01	0.16±0.24	-	-	-
22	H	LYS124	NZ	L94SER	OG	0.14±0.02	0.12±0.07	0.13±0.01	0.13±0.07	0.17±0.22	0.21±0.10
23	H	ASP26	OD1	L31SER	OG	0.09±0.14	-	0.09±0.09	0.37±0.55	0.26±0.10	0.34±0.58
24	H	ARG125	NH2	H99GLU	OE2	-	-	-	1.26±0.50	0.39±0.62	1.26±1.73
25	H	ARG125	O	L31SER	OG	-	-	-	1.02±0.42	0.27±0.08	1.09±1.00
26	S	ASP61		H31ARG		-	-	-	0.47±0.48	1.06±0.04	0.23±0.40
27	H	THR127	OG1	L31SER	OG	-	-	-	0.98±0.43	0.21±0.07	0.96±0.86
28	H	ARG125	O	L30SER	OG	-	-	-	0.54±0.79	0.04±0.03	0.35±0.28
29	H	ARG125	NH2	H105GLU	OE1	-	-	-	0.09±0.08	0.17±0.24	0.24±0.32
30	H	ARG125	N	L30SER	OG	-	-	-	0.05±0.06	0.03±0.03	0.17±0.22

The headings I, II, and III denote three different equilibrated complex conformation of durvalumab bound to PD-L1. The superscript numbers on residues (Column 3 and 5) designate the positions of their respective involved residues in sequences of PD-L1 and durvalumab, with serial numbering. The donor- and acceptor-atoms (Column 6) on paratope residues (Column 5), together with their respectively partners (Column 4) on epitope residues (Column 3), contribute to bonds in the binding site. All bonds, which were derived from three independent free and steered MD simulations with equilibrated conformations I, II, and III, respectively, were designated by nonzero values (mean ± SD) of survival ratios and rupture times of bonds. Letter H and S (Column 2) represent hydrogen bond and salt bridge, respectively. *The names of the residues (Column 5) involved in hydrogen bonds or salt bridges with H or L indicating that the residues are on the heavy or the light chain of durvalumab, respectively, and with the number indicating the position of the residue (first three-letter amino acid code). MD, molecular dynamics.

sary to further comprehend residue interactions across the protein interface [20, 31].

A bond's mean survival ratio (ω) was determined by taking the maximum value of the mean survival ratios for the first equilibrated conformations I, II, and III. This allowed for the most accurate calculation possible (Methods, **Table 4**). Twenty-three compounds exhibited distinct thermal stabilities, which were categorized into three groups based on their respective mean survival ratio values: high (0.5-1.0), moderate (0.3-0.55), and low (0-0.3). The stability of the bonds in **Table 3** varied, with the seventh through fifteenth bonds exhibiting moderate stability and the remaining eight (16th-23rd) demonstrating instability. Thermal stabilization of bonds No. 8 and 9 (**Figure 3C** and **3D**) appeared to be greater than those of bonds No. 21 and 22 (**Figure 3E** and **3F**) but lower than those of bonds No. 1 and 4 (**Figure 3A** and **3B**). This is evident in **Figure 3**.

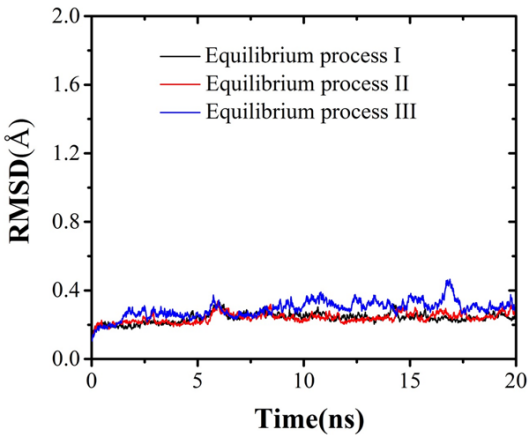

Figure 2. Variation of the RMSD of heavy atoms of durvalumab/PD-L1 complex versus simulation time. I, II, and III denote three independent system equilibrium processes.

To map residues from the paratope to the epitope, high and moderate thermal stability bonds were used. The involvement of the five bonds varied from the first to the fifteenth (**Table 3**). Thirteen residues were sorted using a threshold value of 0.3: ASP26, GLU58, GLU60, ARG113, and ARG115 on PD-L1 and H52LYS, H53GLN, H57GLU, H103PHE, H113ARG, L28ARG, L31SER, and L92TYR on durvalumab (**Figure 4**). ASP26, ARG113, and ARG125 located on PD-L1 were determined to play a crucial role in the interaction between PD-L1 and PD-1, demonstrating that the antibody durvalumab exhibited steric hindrance. The comparison between the crystal structures indicated that four residues were sorted (GLU60 on PD-L1 and L31SER, H53GLN, and H113ARG on durvalumab), and two residues (LYS124 on PD-L1 and L94SER on durvalumab) were missed. This implies that the complex underwent conformational changes in MD simulations. The unstable bonds ruptured (i.e., No. 2 hydrogen bond in **Table 2**), whereas new bonds (i.e., No. 14 bond in **Table 3**) formed during this process.

Epitope-to-paratope residues detected in the guided MD simulations

Paratope and epitope residues were mapped using the mechanical stability of bonds being assessed in a manner analogous to the thermal stability, as shown by the bond's survival ratios [20]. The rupture times of the bonds, as shown in **Table 3**, were determined using guided MD simulations. These simulations were conducted thrice for each of the three equilibrated conformations (Methods). Random characteristics and the dependence of bonds on the initial state were also detected, and these phenomena mirrored those observed in the free MD simulations. As illustrated in **Table 3**, the development of the tenth bond was noticed only in the simulations that were conducted for equilibrated conformation III, whereas the second and third bonds were observed only in the simulations that pertained to equilibrated conformations I and III, respectively.

The normalized mean rupture time (α) of each bond was calculated once the data were standardized (**Table 4**; Methods). The normalized mean rupture times for each bond observed through MD simulations were used to classify the bonds into three distinct types: strong, moderate, and feeble mechanically stable (varying between 0 and 0.3, 0.3 and 0.55, 0.55 and 1.0, respectively). As an illustration, bonds 21 and 22 ruptured rapidly compared with the others; bonds 1 and 4 maintained their integrity for a longer duration than bonds 8 and 9 (**Figure 5**).

Thirteen bonds, including the first to fifth, eighth to ninth, twelfth, sixteenth, and twenty-fourth to twenty-seventh bonds in **Table 3**, had α greater than 0.3, indicating good and moderate mechanical stability. With these links, 14 residues were expected to represent paratopes and epitopes; these included eight residues on durvalumab (H31ARG, H52LYS, H57GLU, H99GLU, H103PHE, H113ARG, L31SER, and L92TYR) and six residues on PD-L1 (ASP26, GLU58, ASP61, ARG113, ARG125, and THR127) (**Table 4**; **Figure 4**). Three residues (GLU60 on PD-L1 and H53GLN and L28ARG on durvalumab) were overlooked in the guided MD simulations, according to a comparison with the findings from free MD simulations. Additionally, ASP61 and THR127 on PD-L1 and H31ARG and H99GLU on durvalumab were singled out for investigation. This indicated that a bond may be mechanically stable but not thermally stable (i.e., No. 24-27 bonds in **Table 3**) and vice versa (i.e., No. 14 bonds in **Table 3**).

Mapping of PD-L1/durvalumab complex paratopes to epitopes using the H-bond stabilization index

The thermal and mechanical stabilities of a bond, or HBSI, were calculated by taking the

Table 4. Mean survival ratio (ω), normalized mean rupture time (α) and HBSI values of bonds

Rank	Bond No.#	ω	α	HBSI	Interaction residue pairs	
					PD-L1	Durvalumab*
1	2	0.96	1.00	1.00	GLU58	H52LYS
2	4	0.86	0.98	0.98	ARG113	H57GLU
3	1	0.97	0.91	0.97	ARG113	H57GLU
4	3	0.94	0.97	0.97	ARG113	H113ARG
5	5	0.79	0.69	0.79	ARG125	L92TYR
6	6	0.75	0.14	0.75	ARG125	H103PHE
7	9	0.44	0.57	0.57	ARG125	H103PHE
8	16	0.29	0.55	0.55	ASP26	L31SER
9	12	0.39	0.49	0.49	GLU58	H52LYS
10	7	0.48	-	0.48	ASP26	L28ARG
11	8	0.46	0.37	0.46	GLU58	H52LYS
12	10	0.42	0.05	0.42	ASP26	L28ARG
13	11	0.4	-	0.4	ASP26	L28ARG
14	13	0.39	0.16	0.39	ASP26	L31SER
15	14	0.38	0.09	0.38	GLU60	H53GLN
16	24	-	0.38	0.38	ARG125	H99GLU
17	25	-	0.33	0.33	ARG125	L31SER
18	15	0.32	-	0.32	ARG113	H57GLU
19	26	-	0.32	0.32	ASP61	H31ARG
20	27	-	0.30	0.3	THR127	L31SER
21	17	0.29	-	0.29	ASP26	L28ARG
22	18	0.27	-	0.27	ASP26	L28ARG
23	20	0.23	0.25	0.25	TYR123	H50ASN
24	19	0.24	-	0.24	ARG113	H57GLU
25	21	0.16	-	0.16	ASP26	L31SER
26	28	-	0.16	0.16	ARG125	L30SER
27	22	0.14	0.06	0.14	LYS124	L94SER
28	23	0.09	0.11	0.11	ASP26	L31SER
29	29	-	0.07	0.07	ARG125	H105GLU
30	30	-	0.05	0.05	ARG125	L30SER

#The bond no. in column 2 were same as those in **Table 3**. ω and α (Column 3 and 4) express the thermal and mechanical stabilities of the bonds detected from free and steered MD simulations thrice with three different equilibrated conformations (Method). HBSI expresses the index of hydrogen bond stabilization (Method). *The names of the residues (Column 7) involvec in hydrogen bonds or salt bridges with H or L indicating that the residues are on the heavy or the light chain of durvalumab, respectively, and with the number indicating the position of the residue (first three-letter amino acid code). MD, molecular dynamics.

maximum of the mean survival ratio and the normalized mean rupture time of each discovered bond to synthetically score. This information was published in our earlier study on the antithrombotic antibody 6B4 [20]. By comparing the HBSI values of each bond, with ranges of 0-0.3, 0.3-0.55, and 0.55-1.0, all the bonds were categorized into three groups: low, moderate, and high stability (**Table 4**).

According to **Table 4**, it was anticipated that the top twenty bonds would have a stability level ranging from moderate to high because their HBSI ratings ranged from 0.3 to 1. Seventeen residues, namely, ASP26, GLU58, GLU60, ASP61, ARG113, ARG125, and THR127 on PD-L1 and H31ARG, H52LYS, H53GLN, H57GLU, H99GLU, H103PHE, H113ARG, L28ARG, L31SER, and L92TYR on durvalumab, were involved in the stable bonds (**Figure 4**). Thermally or mechanically stable bonds were sorted using HBSI, which provided all possible interaction-residue pairs in the interface.

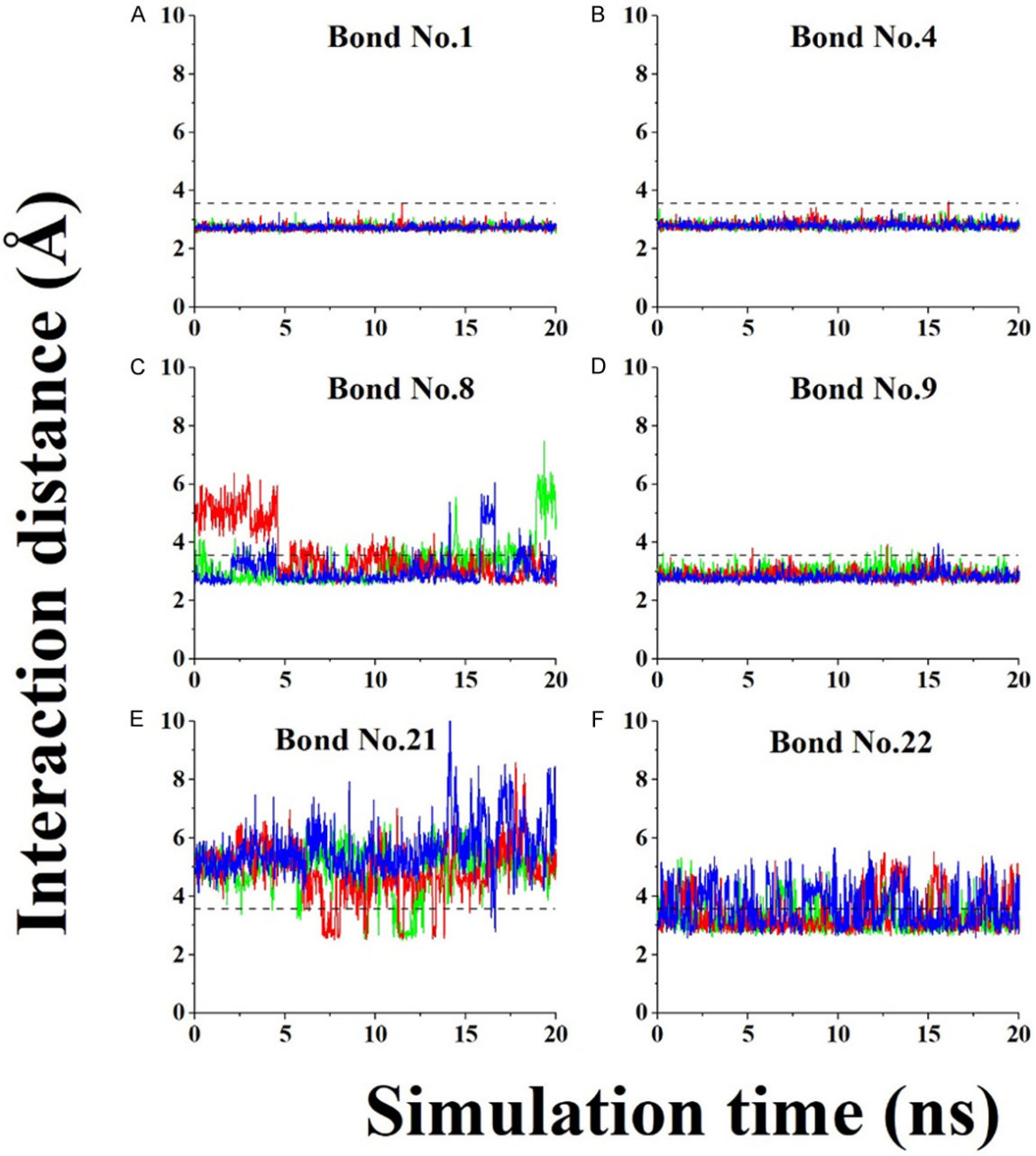

Figure 3. Time courses of interatomic distances of six representative bonds in binding site of durvalumab/PD-L1 complex. The interatomic distances of six representative bonds were plotted against simulation time, where the interatomic distances were from donors to their respective acceptors for three hydrogen bonds. The hydrogen bonds were simulated with the initial conformation I (FMD1_1~FMD1_3). The black dashed line expresses the distance cut-off of 0.35 nm beyond which the bonds breaks, and the blue, green and red lines exhibit the variation of interatomic distances of a bond against simulation time for thrice-repeat independent free MD simulations, respectively. The thermal stabilizations of the No. 8 and 9 bonds seemed to be higher than those of the No. 21 and 22 bonds but lower than those of the No. 1 and 4 bonds. Significant differences in the thrice-repeat independent simulations showed a random behavior of intermolecular interactions.

Discussion

Molecular dynamics (MD) simulations accompanied by HBSI are useful tools for mapping paratope residues to epitope residues for antibodies [20, 23, 24]. Durvalumab is an FDA-approved human monoclonal antibody that targets PD-L1, but the molecular basis of its dur-

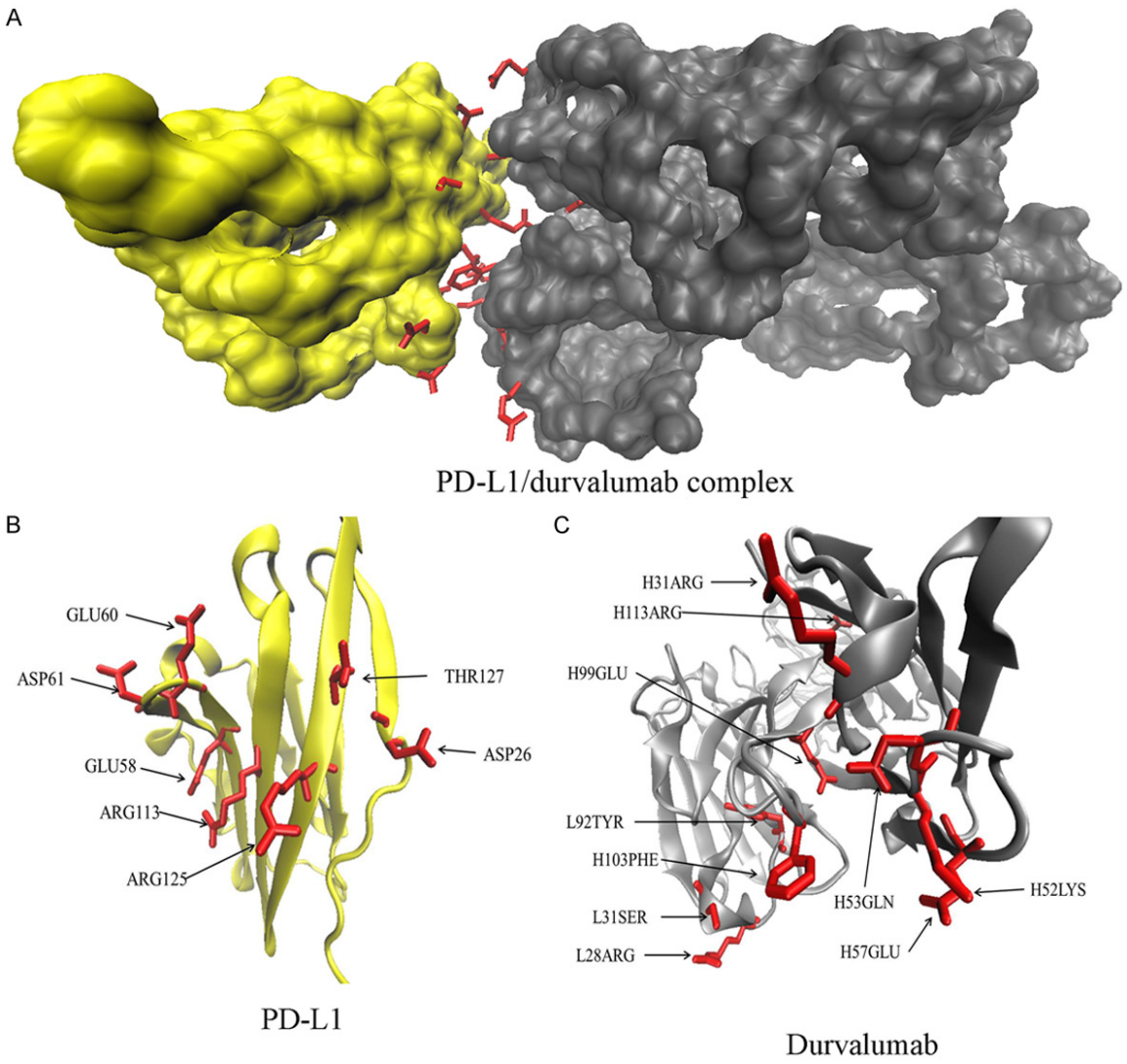

Figure 4. Predicted interaction residues on the interface of the durvalumab/PD-L1 complex by molecular dynamics simulation. A. The durvalumab/PD-L1 complex; B. The predicted epitope residues on PD-L1; C. The predicted paratope residues on durvalumab. PD-L1 is shown in yellow and durvalumab is presented in gray. Predicted residues were shown in red with name labelled. All interaction residues on the interface of durvalumab/PD-L1 complex were predicted in terms of the mean survival ratio, normalized mean rupture time, or HBSI index.

valumab-based anti-PD-L1 reactivity and binding characteristics remains unclear [17]. Using MD simulations as the basis for a unique computational approach [20], the paratope-to-epitope residues of the durvalumab/PD-L1 complex were mapped. Seventeen residues, including ASP26, GLU58, GLU60, ASP61, ARG113, ARG125, and THR127 on PD-L1 and H31ARG, H52LYS, H53GLN, H57GLU, H99GLU, H103PHE, H113ARG, L28ARG, L31SER, and L92TYR on durvalumab, were predicted to play an important role in durvalumab binding to PD-L1. Eight residues (GLU60, ASP61, and THR127 on PD-L1 and L31SER, H99GLU, H53GLU, H31ARG, and H113ARG on durvalumab) were newly found, whereas two residues (LYS124 on PD-L1 and L94SER on durvalumab) proved nonessential for complexation, as compared with the results of the crystal structure investigation. ASP26, ARG113, and ARG125 are essential for PD-L1 to bind with PD-1 [32] (**Table 1**), implying that durvalumab prevents PD-1 from interacting with PD-L1 because of its steric hindrance. Our findings provide potential targets for antibody optimization and suggest that MD simulations are effective in mapping paratopes to epitopes [21, 22].

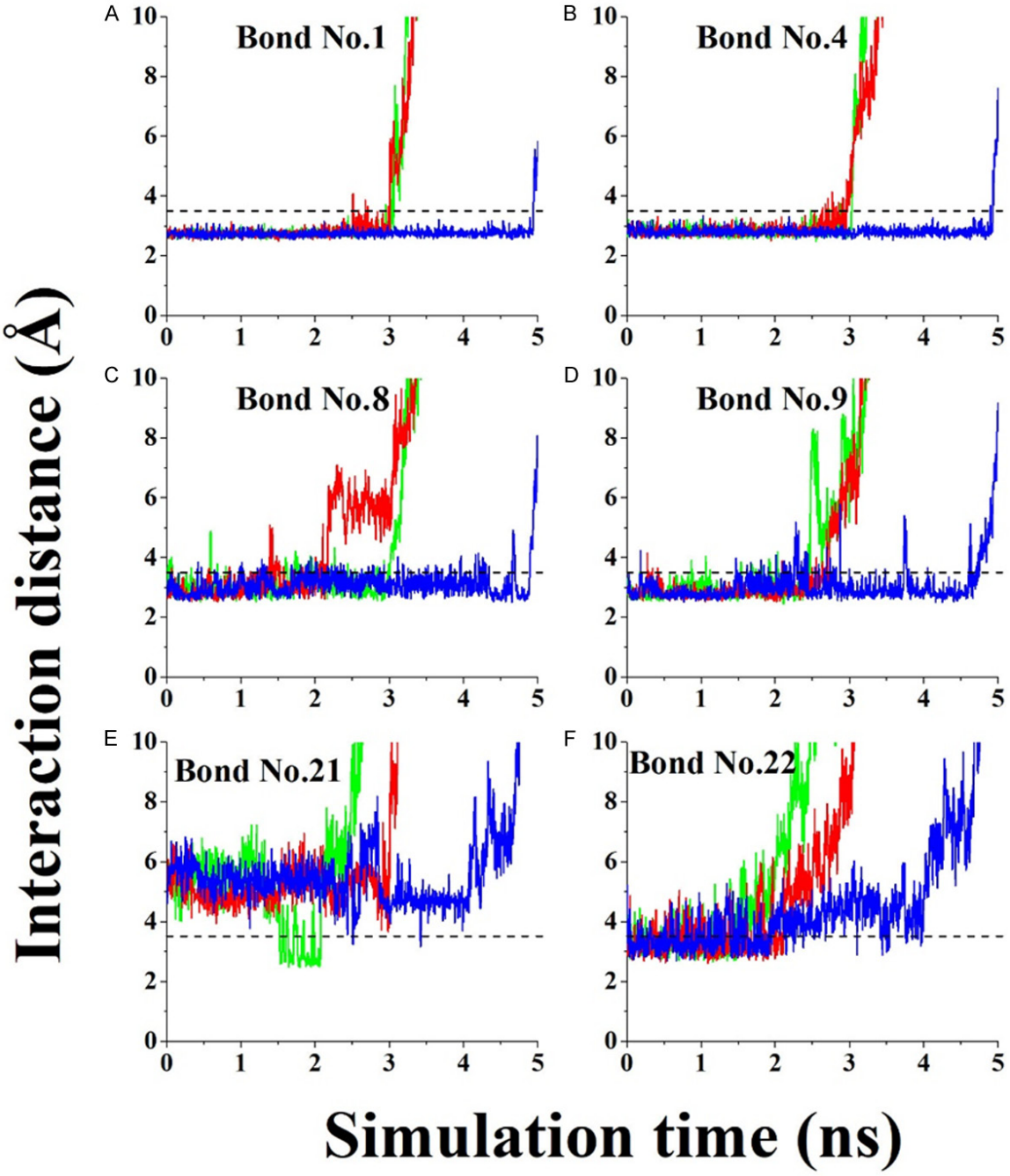

Figure 5. Variation of interatomic distance versus steered simulation time. The interatomic distances of the six representative bonds under stretching were plotted against simulation time, where all descriptions for line types, bonds and their lengths are same as those in **Figure 2**. These time courses of interatomic distances showed that, the No. 21 and 22 bonds were very quickly ruptured, in comparison to others, in which the No. 1 and 4 bonds maintained longer duration than the No. 8 and 9 bonds.

Significant plasticity within PD-1 was observed in the interactions between PD-1, PD-L1, pembrolizumab,, and nivolumab [23, 30]. MD simulation is a useful tool for investigating conformational changes in antibodies because it can reproduce the thermodynamic properties of biomolecules and elucidate all binding-pocket configurations. For example, an open-to-closed switch of the CC' loop of PD-1 is observed upon PD-L1 binding and stabilizes the complex in MD simulations. The moderate stability of the intramolecular hydrogen bonds between SER71 and

THR120 allows the CC' loop to sample the open and closed states in apo-PD-1. The binding of PD-L1 accelerates the open-to-closed switch and locks the CC' loop in the closed state through four newly formed intermolecular hydrogen bonds. Thus, a complex binding mechanism between PD-1 and PD-L1 has been suggested, in which conformational selection and induced fit theories play a role [30]. Moreover, two PD-1-targeting antibodies, GY-5 and GY-14, mainly bind to the flexible FG loop of PD-1, which adopts substantially varied conformations upon binding and contributes to multiple interactions with PD-L1 [33]. MD simulations also revealed that pembrolizumab induces an unexpected conformational change in the CC' loop of PD-1, called "overturned" [34]. In 2020, Liu *et al*. performed MD simulations for the nivolumab/PD-1 complex and proposed a two-step binding model in which the interface of the nivolumab/PD-1 complex switches to a stronger binding state with the help of the N-terminal loop of PD-1. The N-terminal loop of PD-1 prefers to bind with nivolumab to stabilize the complex interface between the IgV domain and nivolumab. Furthermore, the binding of the N-terminal loop with nivolumab induces the interaction between the IgV domain and nivolumab [23]. Moreover, long-term MD simulations were successfully conducted for the avelumab/PD-L1 and toripalimab/PD-1 complexes to detect the key residues regulating binding [25, 35]. Thus, the molecules undergo different conformational changes in the binding process, and MD simulation is an effective method for providing detailed interface information for the complex. The key residues mapped in this study are potential targets for antibody design in the future.

Three salt bridges and four hydrogen bonds were observed across the contact in the static crystal structure, involving five epitope residues (ASP26, GLU58, ARG113, LYS124, and ARG125) on PD-L1 and six paratope residues (L28ARG, H52LYS, H57GLU, L94SER, L92TYR, and H103PHE) on durvalumab. However, the hydrogen bond between LYS124 and L94SER (No. 2 in **Table 2**) was unstable, so these two residues were excluded from the MD simulations. Furthermore, some new interaction-residue pairs were discovered in the simulations, such as the No. 14 and 26 bonds in **Table 3**. Notably, the interaction-residue pairs have different thermal and mechanical stabilities. For example, the No. 7 bond only appeared in free MD simulations, whereas No. 23-30 bonds only appeared in guided MD simulations (**Table 3**). The results of the guided MD simulations revealed more new bonds at the interface, suggesting that more priority should be given to the mechanical stability of the bonds. The reason might be that the mechanical stretch could cross the barrier of conformational transformation to better mimic the dynamic process of protein-protein binding.

In summary, this study performed durvalumab/PD-L1 complex residue mapping from paratope to epitope using the suggested computer-aided method. However, the predicted residues should be further confirmed using mutagenesis, and this strategy could be improved by extending the simulation time or by conducting further parallel simulations.

Disclosure of conflict of interest

None.

Address correspondence to: Wenjian Tu, School of Biology and Biological Engineering, South China University of Technology, Higher Education MegaCenter, No. 382 East Outer Loop Road, Guangzhou 510006, Guangdong, China. E-mail: tuwj2166@163.com

References

[1] Callahan MK, Postow MA and Wolchok JD. Targeting T cell co-receptors for cancer therapy. Immunity 2016; 44: 1069-1078.

[2] Li Y, Li F, Jiang F, Lv X, Zhang R, Lu A and Zhang G. A mini-review for cancer immunotherapy: molecular understanding of PD-1/PD-L1 pathway & translational blockade of immune checkpoints. Int J Mol Sci 2016; 17: 1151.

[3] Pardoll DM. The blockade of immune checkpoints in cancer immunotherapy. Nat Rev Cancer 2012; 12: 252-264.

[4] Zak KM, Grudnik P, Magiera K, Domling A, Dubin G and Holak TA. Structural biology of the immune checkpoint receptor PD-1 and its ligands PD-L1/PD-L2. Structure 2017; 25: 1163-1174.

[5] Freeman GJ, Long AJ, Iwai Y, Bourque K, Chernova T, Nishimura H, Fitz LJ, Malenkovich N, Okazaki T, Byrne MC, Horton HF, Fouser L, Carter L, Ling V, Bowman MR, Carreno BM, Collins M, Wood CR and Honjo T. Engagement of the PD-1 immunoinhibitory receptor by a novel

B7 family member leads to negative regulation of lymphocyte activation. J Exp Med 2000; 192: 1027-1034.
[6] Okazaki T, Chikuma S, Iwai Y, Fagarasan S and Honjo T. A rheostat for immune responses: the unique properties of PD-1 and their advantages for clinical application. Nat Immunol 2013; 14: 1212-1218.
[7] John LB, Devaud C, Duong CP, Yong CS, Beavis PA, Haynes NM, Chow MT, Smyth MJ, Kershaw MH and Darcy PK. Anti-PD-1 antibody therapy potently enhances the eradication of established tumors by gene-modified T cells. Clin Cancer Res 2013; 19: 5636-5646.
[8] Zak KM, Kitel R, Przetocka S, Golik P, Guzik K, Musielak B, Domling A, Dubin G and Holak TA. Structure of the complex of human programmed death 1, PD-1, and its ligand PD-L1. Structure 2015; 23: 2341-2348.
[9] Ivashko IN and Kolesar JM. Pembrolizumab and nivolumab: PD-1 inhibitors for advanced melanoma. Am J Health Syst Pharm 2016; 73: 193-201.
[10] Lee JY, Lee HT, Shin W, Chae J, Choi J, Kim SH, Lim H, Won Heo T, Park KY, Lee YJ, Ryu SE, Son JY, Lee JU and Heo YS. Structural basis of checkpoint blockade by monoclonal antibodies in cancer immunotherapy. Nat Commun 2016; 7: 13354.
[11] Leventakos K and Mansfield AS. Advances in the treatment of non-small cell lung cancer: focus on nivolumab, pembrolizumab, and atezolizumab. BioDrugs 2016; 30: 397-405.
[12] Sidaway P. Urological cancer: atezolizumab: an alternative to cisplatin? Nat Rev Clin Oncol 2017; 14: 139.
[13] Rittmeyer A, Barlesi F, Waterkamp D, Park K, Ciardiello F, von Pawel J, Gadgeel SM, Hida T, Kowalski DM, Dols MC, Cortinovis DL, Leach J, Polikoff J, Barrios C, Kabbinavar F, Frontera OA, De Marinis F, Turna H, Lee JS, Ballinger M, Kowanetz M, He P, Chen DS, Sandler A and Gandara DR; OAK Study Group. Atezolizumab versus docetaxel in patients with previously treated non-small-cell lung cancer (OAK): a phase 3, open-label, multicentre randomised controlled trial. Lancet 2017; 389: 255-265.
[14] Lee HT, Lee JY, Lim H, Lee SH, Moon YJ, Pyo HJ, Ryu SE, Shin W and Heo YS. Molecular mechanism of PD-1/PD-L1 blockade via anti-PD-L1 antibodies atezolizumab and durvalumab. Sci Rep 2017; 7: 5532.
[15] Massard C, Gordon MS, Sharma S, Rafii S, Wainberg ZA, Luke J, Curiel TJ, Colon-Otero G, Hamid O, Sanborn RE, O'Donnell PH, Drakaki A, Tan W, Kurland JF, Rebelatto MC, Jin X, Blake-Haskins JA, Gupta A and Segal NH. Safety and efficacy of durvalumab (MEDI4736), an anti-programmed cell death ligand-1 immune checkpoint inhibitor, in patients with advanced urothelial bladder cancer. J Clin Oncol 2016; 34: 3119-3125.
[16] Carter PJ. Potent antibody therapeutics by design. Nat Rev Immunol 2006; 6: 343-357.
[17] Tan S, Liu K, Chai Y, Zhang CW, Gao S, Gao GF and Qi J. Distinct PD-L1 binding characteristics of therapeutic monoclonal antibody durvalumab. Protein Cell 2018; 9: 135-139.
[18] Gershoni JM, Roitburd-Berman A, Siman-Tov DD, Tarnovitski Freund N and Weiss Y. Epitope mapping: the first step in developing epitope-based vaccines. BioDrugs 2007; 21: 145-156.
[19] Moroni E, Paladino A and Colombo G. The dynamics of drug discovery. Curr Top Med Chem 2015; 15: 2043-2055.
[20] Fang X, Fang Y, Liu L, Liu G and Wu J. Mapping paratope on antithrombotic antibody 6B4 to epitope on platelet glycoprotein Ibalpha via molecular dynamic simulations. PLoS One 2012; 7: e42263.
[21] Adcock SA and McCammon JA. Molecular dynamics: survey of methods for simulating the activity of proteins. Chem Rev 2006; 106: 1589-1615.
[22] Plattner N, Doerr S, De Fabritiis G and Noe F. Complete protein-protein association kinetics in atomic detail revealed by molecular dynamics simulations and Markov modelling. Nat Chem 2017; 9: 1005-1011.
[23] Liu W, Jin H, Chen T, Zhang G, Lai S and Liu G. Investigating the role of the N-terminal loop of PD-1 in binding process between PD-1 and nivolumab via molecular dynamics simulation. Front Mol Biosci 2020; 7: 574759.
[24] Liu W, Liu G, Zhou H, Fang X, Fang Y and Wu J. Computer prediction of paratope on antithrombotic antibody 10B12 and epitope on platelet glycoprotein VI via molecular dynamics simulation. Biomed Eng Online 2016; 15 Suppl 2: 152.
[25] Boisgerault N and Bertrand P. Inside PD-1/PD-L1,2 with their inhibitors. Eur J Med Chem 2023; 256: 115465.
[26] Humphrey W, Dalke A and Schulten K. VMD: visual molecular dynamics. J Mol Graph 1996; 14: 33-8, 27-8.
[27] Phillips JC, Braun R, Wang W, Gumbart J, Tajkhorshid E, Villa E, Chipot C, Skeel RD, Kale L and Schulten K. Scalable molecular dynamics with NAMD. J Comput Chem 2005; 26: 1781-1802.
[28] Whitford PC, Noel JK, Gosavi S, Schug A, Sanbonmatsu KY and Onuchic JN. An all-atom structure-based potential for proteins: bridging minimal models with all-atom empirical forcefields. Proteins 2009; 75: 430-441.
[29] Konermann L, Aliyari E and Lee JH. Mobile protons limit the stability of salt bridges in the gas

phase: implications for the structures of electrosprayed protein ions. J Phys Chem B 2021; 125: 3803-3814.
[30] Liu W, Huang B, Kuang Y and Liu G. Molecular dynamics simulations elucidate conformational selection and induced fit mechanisms in the binding of PD-1 and PD-L1. Mol Biosyst 2017; 13: 892-900.
[31] Zeiske T, Stafford KA, Friesner RA and Palmer AG 3rd. Starting-structure dependence of nanosecond timescale intersubstate transitions and reproducibility of MD-derived order parameters. Proteins 2013; 81: 499-509.
[32] Sheinerman FB and Honig B. On the role of electrostatic interactions in the design of protein-protein interfaces. J Mol Biol 2002; 318: 161-177.
[33] Chen D, Tan S, Zhang H, Wang H, He W, Shi R, Tong Z, Zhu J, Cheng H, Gao S, Chai Y, Qi J, Xiao M, Yan J and Gao GF. The FG loop of PD-1 serves as a "hotspot" for therapeutic monoclonal antibodies in tumor immune checkpoint therapy. iScience 2019; 14: 113-124.
[34] Roither B, Oostenbrink C, Pfeiler G, Koelbl H and Schreiner W. Pembrolizumab induces an unexpected conformational change in the CC'-loop of PD-1. Cancers (Basel) 2020; 13: 5.
[35] Huyghe N, Benidovskaya E, Stevens P and Van den Eynde M. Biomarkers of response and resistance to immunotherapy in microsatellite stable colorectal cancer: toward a new personalized medicine. Cancers (Basel) 2022; 14: 2241.